Autonomous Isotropy-Based Integrity Using GPS and GLONASS

M. Azaola, D. Calle, A. Mozo, R. Píriz, *GMV, Spain*

BIOGRAPHY

Miguel Azaola has a Master of Science in Mathematics from the University Complutense of Madrid and a Ph.D. in geometry and topology from the University of Cantabria (at Santander, Spain). He has worked at GMV since 2001 as an engineer in several GNSS projects related to both the ground and user segments. Since 2005 he has been involved in user segment R&D activities at engineering and management levels.

Ricardo Píriz has a Master of Science in Aerospace Engineering, from the Universidad Politécnica de Madrid, Spain. He is the *magicGNSS* Product Manager within the GNSS Business Unit of GMV.

David Calle has a Master of Science in Computer Engineering, from the Universidad de Salamanca, Spain. He works as Web 2.0 and Human-Computer Interaction specialist at GMV.

Álvaro Mozo has a Master of Science in Aeronautical Engineering, from the Universidad Politécnica de Madrid, Spain. He is Head of the GNSS Algorithms and Products Division within the GNSS Business Unit of GMV.

ABSTRACT

After the launch of three new GLONASS satellites on March 1, 2010, the Russian constellation consists now of more than 20 operational satellites. A total of three triple-spacecraft launches are planned to take place this year. The 'GNSS constellation', including GPS and GLONASS, provides currently more than 50 usable satellites. For the GNSS user this means that up to 18 GPS+GLONASS satellites can be simultaneously visible in open-sky areas. This represents an increase of around 60% in satellite availability with respect to the GPS-only scenario.

Most integrity provision techniques, either autonomous or assisted (e.g., by SBAS or GBAS) have been conceived for the civil aviation framework. Due to the harsh conditions found in urban environments, such as heavy multipath, and very especially non-line-of-sight (NLOS) multipath, some of the assumptions made for civil aviation integrity do not hold. Isotropy-Based Protection Level (IBPL) is an autonomous integrity algorithm specifically developed by GMV to face the challenges associated to urban environments. Nonetheless, IBPL turns out to be a flexible integrity provision technique that performs well in all environments, and hence is suitable for a wide variety of applications including civil aviation. IBPL performance in terms of typical Protection Level size depends strongly on the number of satellites available, and hence the new GPS+GLONASS scenario implies a dramatic improvement with respect to the usual GPS-only solution.

In order to validate the IBPL concept it is necessary to know the *true* receiver antenna position. By *true* position we mean coordinates that are known to have an error several orders of magnitude smaller than the standard pseudorange-based position used in IBPL.

Precise Point Positioning (PPP) is a relatively new positioning technique providing centimeter-level error. PPP processes pseudorange and carrier-phase measurements from a single user receiver, using detailed physical models and corrections, and precise GNSS orbit and clock products calculated beforehand (for example products from IGS, the *International GNSS Service*) [1]. PPP is different from other precise-positioning approaches like RTK in that no reference stations are needed in the vicinity of the user receiver. The only observation data that must be processed are measurements from the user receiver.

Another advantage of PPP is that since the GNSS orbit and clock products are by nature global, the PPP solutions are also global, i.e., the PPP approach works for a receiver located anywhere on or above the Earth surface, and the resulting position is referred to a well-known terrestrial reference frame (normally ITRF). PPP can be applied at post-processing level and also in real-time applications, provided that real-time input orbits and clocks are available.

This paper describes the implementation of GPS and GLONASS data processing in the IBPL and PPP modules of the *magicGNSS* web application developed by GMV, including algorithm description and performance analysis, and presents the major results in terms of autonomous integrity statistics using combined GPS+GLONASS real data.

IBPL FUNDAMENTALS

For standard, low-accuracy, stand-alone positioning, the benefits of an extended GNSS constellation is especially important in urban areas where buildings blocking the GNSS signals might reduce the number of visible satellites below the minimum required for a reliable solution. The advantages of multi-constellation GNSS have also been demonstrated in precise positioning applications (Real Time Kinematics and Precise Point Positioning), resulting in higher accuracy and faster convergence. However not so much research has been done in the field of autonomous integrity using real GPS+GLONASS data, mainly because it is only recently that the larger satellite availability has enabled a clear improvement in this area.

The Isotropy-Based Protection Level is a GNSS receiver autonomous integrity monitoring (RAIM) method. It does not implement measurement rejection/exclusion (FDE) mechanisms. Instead it computes a protection level based on the snapshot all-in-view pseudorange-based least squares solution. The protection level is a number that bounds the state estimation error up to a certain probability (or confidence level) $\mathbf{1-\alpha}$. In other words, the probability that the position error exceeds the protection level is $\boldsymbol{\alpha}$ (known also as the integrity risk).

The idea is to use the vector of least squares estimation residuals (or residual vector) as a characterization of the position error. The larger the residual vector, the larger the state estimation error vector, and the relation between both is taken to be linear, so the protection level depends linearly on the size of the residual vector. Of course, the state estimation error depends also on the dilution of precision, so if we are interested, for instance, in a horizontal protection level, we would compute it as

$$HPL = k \cdot \|\boldsymbol{r}\| \cdot HDOP$$

where $\boldsymbol{r}$ is the least squares residual vector and k is the scaling factor that relates the sizes of the residual vector and the state estimation error vector. This constant, which depends on the target integrity risk α, is called the *isotropy confidence ratio* and is defined so as to ensure that the state estimation error $\boldsymbol{\delta}$ (or, more precisely, its image through the least squares design matrix $\boldsymbol{G}$) is bounded by the size of the residual vector times k with the required probability $1-\alpha$:

$$P(\|\boldsymbol{G}\cdot\boldsymbol{\delta}\| \le k \cdot \|\boldsymbol{r}\|) \ge 1-\alpha \qquad \text{Eq. 1}$$

For computing k from the preceding relation, it is assumed that the measurement error vector has an isotropic distribution in the measurement space (and hence the name for the constant k and for the method itself), that is, it can point in any direction of the measurement space with the same probability. Note that this does not imply any particular distribution of the individual measurement errors (e.g. Gaussian), nor that they are unbiased or have known variance. Individual errors can be arbitrarily large or biased as long as they define an error vector that has the same a priori probability of pointing in any direction of the measurement space. This a priori probability must be understood as the relative frequency of the error vector pointing in each possible direction when the system is left running for an infinite time.

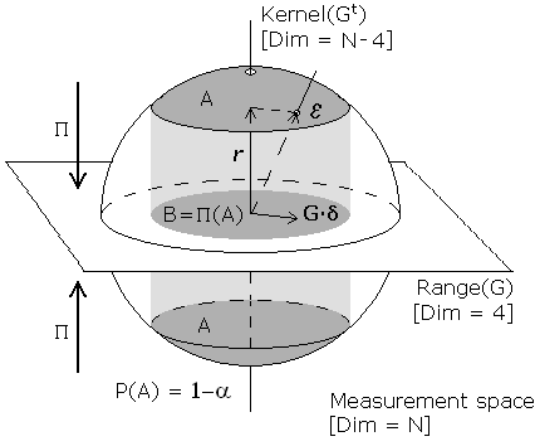

Figure 1: The IBPL concept

Isotropy implies that the pointing direction of the error vector defines a uniform distribution in the centered sphere of the N-dimensional measurement space (see Figure 1). On the other hand, the condition

$$\|\boldsymbol{G}\cdot\boldsymbol{\delta}\| \le k \cdot \|\boldsymbol{r}\| \qquad \text{Eq. 2}$$

establishes a maximum value (k) for the ratio

$$\frac{\|\boldsymbol{G}\cdot\boldsymbol{\delta}\|}{\|\boldsymbol{r}\|}$$

The vectors $\boldsymbol{G}\cdot\boldsymbol{\delta}$ and $\boldsymbol{r}$ constitute an orthogonal decomposition of the measurement error vector $\boldsymbol{\varepsilon}$ in the measurement space, $\boldsymbol{G}\cdot\boldsymbol{\delta}$ being in the range of the matrix $\boldsymbol{G}$ and $\boldsymbol{r}$ being in the null space (that is, the kernel) of $\boldsymbol{G}^t$, so the preceding ratio describes the slope of $\boldsymbol{\varepsilon}$ with respect to the range of $\boldsymbol{G}$ (see Figure 1). The ratio is actually the inverse of the slope.

Hence, for each fixed value of k, Eq. 2 defines a region of the sphere (called A in Figure 1), which is the region of possible pointing directions of $\boldsymbol{\varepsilon}$ for which Eq. 2 is satisfied. If we take k so that the area of A is a fraction $1-\alpha$ of the total area of the sphere, then Eq. 1 will also be satisfied (provided that the isotropy assumption holds). Equivalently, the projection of A into the range of $\boldsymbol{G}$ defines another region B which contains the vector $\boldsymbol{G}\cdot\boldsymbol{\delta}$ with the required probability $1-\alpha$.

Now we observe that Eq. 2 is equivalent to:

$$\boldsymbol{\delta}^t\cdot\boldsymbol{G}^t\boldsymbol{G}\cdot\boldsymbol{\delta}\leq(k\cdot\|\boldsymbol{r}\|)^2 \qquad \text{Eq. 3}$$

Therefore, choosing k so that Eq. 1 holds, which means that Eq. 2 holds with probability $1-\alpha$, we have that also Eq. 3 holds with probability $1-\alpha$. But Eq. 3 defines a solid ellipsoid in the position-clock domain, and Eq. 1 says that the state estimation error $\boldsymbol{\delta}$ is contained in this ellipsoid with probability $1-\alpha$, so if d is the ellipsoid's semi-major axis, then

$$\|\boldsymbol{\delta}\|\leq d$$

holds also with probability $1-\alpha$ or higher (by taking the semi-major axis we are being conservative). Furthermore, if we are interested in the horizontal component of the position error we can project the ellipsoid to the horizontal plane, obtaining a solid ellipse which contains the horizontal component of the position error, $\boldsymbol{\delta}_H$, with the same or even higher probability. If d_H is the semi-major axis of the ellipse, then we also have

$$\|\boldsymbol{\delta}_H\|\leq d_H$$

with probability $1-\alpha$ or higher. It can be shown that d_H is always smaller than $k\cdot\|\boldsymbol{r}\|\cdot HDOP$, and hence:

$$P(\|\boldsymbol{\delta}_H\|\leq k\cdot\|\boldsymbol{r}\|\cdot HDOP)\geq 1-\alpha$$

Therefore we take the horizontal protection level to be $k\cdot\|\boldsymbol{r}\|\cdot HDOP$ (as we stated in our original equation, at the beginning of this section) which guarantees the target integrity risk as long as the isotropy assumption holds.

ADDITIONAL REMARKS ABOUT IBPL

Once the basic idea behind the IBPL concept has been described, it is worth making some further observations:

- A vertical protection level with the same integrity risk can be analogously obtained (using the same value of k) as:

$$VPL=k\cdot\|\boldsymbol{r}\|\cdot VDOP$$

- A slight improvement (that is, a smaller protection level but still covering with probability $1-\alpha$ or higher) can be obtained in the horizontal case if instead of HDOP we take the semi-major axis of the ellipse obtained as the horizontal projection of the ellipsoid defined by:

$$\boldsymbol{\delta}^t\cdot\boldsymbol{G}^t\boldsymbol{G}\cdot\boldsymbol{\delta}\leq 1$$

- In the case of dual constellation positioning, to which this paper is devoted, the dimension of the state space is not 4 but 5, since an additional clock parameter accounting for the inter-system bias needs to be estimated (unless provided by an external source). This yields slightly different values of k than the 4-state case, but the method works the same.

- The value of k does not depend only on the target integrity risk α, but also on the number of measurements N, which defines the dimension of the measurement space and hence of the sphere used to compute k. Actually, as noticed in the previous bullet, k also depends on the number M of parameters being estimated (5 in this paper):

$$k=k(\alpha,M,N)$$

- In a typical positioning application where α and M are fixed, k can be pre-computed and tabulated for different values of N, so that calculating protection levels is just a matter of looking up in a table and adding two extra multiplications to the least squares estimation routine. More generally, k can be pre-computed and tabulated also for different values of M, and even of α.

- The isotropy concept, in order to be well defined, requires that a particular reference frame of the measurement space is chosen. The correct choice so that our construction works correctly would be an orthonormal reference frame all whose basic vectors are either contained in the range of $\boldsymbol{G}$ or in its orthogonal complement. This implies that, even when there is a biased satellite (or several of them), the isotropy assumption is not necessarily violated, since the direction of the bias in the measurement space depends on the particular satellite geometry and hence is still widely variable in time.

- Biases that are common to all satellites (e.g. tropospheric delay to some extent) are a clear source of anisotropy, but this still does not invalidate the method; it can be shown that, as

the common part of the bias is absorbed by the receiver clock estimate, there is no impact at all on position integrity.

More information about IBPL can be found in [2], [3], [4].

PRECISE POINT POSITIONING

In order to validate the IBPL concept it is necessary to know the *true* receiver antenna position. By *true* position we mean coordinates that are known to have an error several orders of magnitude smaller than the standard pseudorange-based position used in IBPL.

High-accuracy positioning at the cm-level can only be achieved combining pseudorange and carrier-phase measurements. Two main techniques are in used nowadays, the well-established RTK (Real Time Kinematics) and the relatively new PPP (Precise Point Positioning).

PPP processes measurements from a single user receiver, using detailed physical models and corrections, and precise GNSS orbit and clock products. PPP differs from other precise-positioning approaches like RTK in that no *reference* or *base* stations are needed in the vicinity of the user. Another advantage is that since the GNSS orbit and clock products are by nature global, the PPP solutions are also global. One disadvantage of PPP, though, is its slow convergence time, in comparison to nearly instantaneous convergence in dual-frequency short-baseline RTK.

The PPP algorithm uses as input pseudorange and carrier phase observations from a dual-frequency receiver, and precise satellite orbits and clocks, in order to calculate precise receiver coordinates and clock. The orbit and clock input products are calculated beforehand by a dedicated software package. The dual-frequency observables are used un-differenced, and combined into the so-called *ionosphere-free combination*. The highlights of the algorithm are described next.

The observations coming from all the satellites are processed together in a process that solves for the different unknowns, namely the receiver coordinates, the receiver clock, the zenith tropospheric delay and the phase ambiguities.

Most implementations of PPP algorithms use a sequential filter in which the process noise for the coordinates is adjusted depending on the receiver dynamics (static or kinematic), the time evolution of the clock is more or less unconstrained (white noise with a high sigma), and the process noise for the tropospheric delay is adjusted to standard tropospheric activity. In the case of phase ambiguities, they are considered as a constant per pass.

Our PPP implementation features a batch algorithm instead, and therefore no process noise has to be modeled. In this case, the receiver clock offset is estimated at every measurement epoch, the coordinates are adjusted for the whole observation interval (in static mode) or per epoch (in kinematic mode), the troposphere is estimated at regular fixed intervals and the ambiguities are also estimated per pass.

The slant tropospheric delay is expressed as a function of the zenith tropospheric delay (which is the parameter that is actually estimated in PPP) through the use of a mapping function.

The precise modeling of Earth dynamics (causing variations of the static receiver coordinates with respect to the terrestrial reference frame) is based on the IERS (International Earth Rotation and Reference Systems Service) recommendations. Such models include solid Earth tides, ocean loading and Earth Rotation. The modeling of the observables includes for instance the offset between the antenna phase center and the satellite center of mass, and the so-called phase wind-up at the receiver.

The accuracy of the satellite clocks and orbits is one of the most important factors affecting the quality of the PPP. Normally, the IGS products [1] (ultra-rapid, rapid, or final) are used due to their high accuracy, however the IGS does not currently provide GLONASS clocks. Furthermore, IGS products have a latency of several hours, which makes them not valid for real-time PPP.

Another relevant factor that affects the PPP performances is the amount (number of satellites in view at each epoch) and quality (noise, multipath) of the observations. For instance, more satellites in view improve the observability of the zenith tropospheric delay. Therefore, a possible way to increase the reliability of this technique is to process GPS and GLONASS observations together.

Given that PPP is not a differential technique, it cannot resolve carrier phase ambiguities and they need to be estimated with the aid of the code measurements. This fact makes the convergence period longer than in other techniques (RTK, for instance), thus requiring longer observation times for static positioning.

REFERENCE PRODUCTS FOR PPP

As mentioned above, the positioning performances of the PPP technique are directly related to the accuracy of the reference GNSS orbit and clock products. Therefore, the generation of precise satellite orbits and clocks in real time becomes a major challenge for enabling a real time positioning service.

GMV has developed an infrastructure for the generation of precise GPS and GLONASS orbits and clocks with very low latency in a first step, and in real time in a second step. The products generated this way are contributed to the IGS Real Time Pilot Project, and are also used to feed GMV's PPP service, part of the web application *magicGNSS* [5], [6].

The product generation is based on an Orbit Determination and Time Synchronisation (ODTS) process, which runs typically every 15 minutes. This process receives as input dual-frequency code and phase measurements collected in real time from a worldwide network of IGS stations, using the NTRIP protocol. Then, they are pre-processed also in real time by a Pre-Processing and Validation module (PPV) and made available to the different algorithms. The high-level layout of the infrastructure is shown in Figure 2.

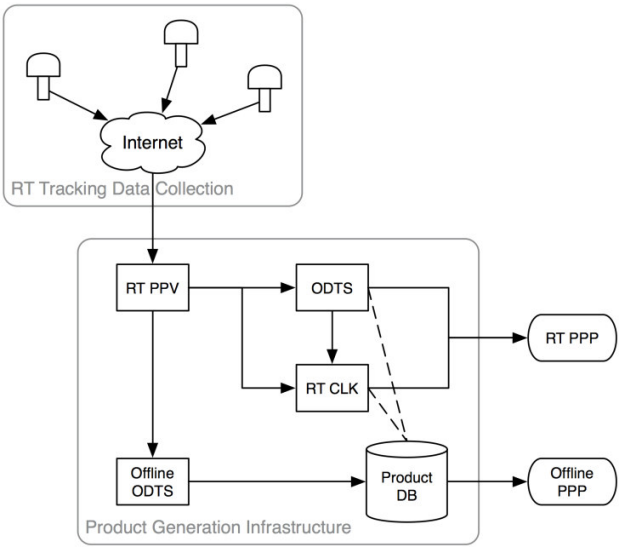

Figure 2: Product Generation Infrastructure Layout

The network, which is represented in Figure 3, provides global coverage and some redundancy to cover the relatively frequent (especially from some stations) outages of the real-time data streams. The color in the figure represents the number of stations that are tracking a satellite when it is flying over a certain point. The red circles show the station positions.

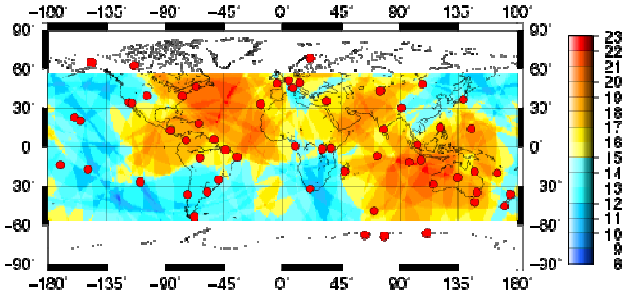

Figure 3: Tracking Station Network

The ODTS processes 2-days of data in every run, and provides updated satellite orbits and other estimated parameters (such as phase ambiguities, station tropospheric zenith delays and Earth orientation parameters).

In parallel to the ODTS, another process estimates the clocks in real time taking as input the observations and the outputs from the last ODTS execution. There is a small latency in the delivery of the clock estimation, which is associated to the time that the algorithm waits for the arrival of the measurements from the station through the Internet; typically one or two seconds.

The GPS and GLONASS satellites are processed together, in order to ensure a consistent solution. It is necessary to estimate an *inter-channel bias* when processing GLONASS data. This must be done in order to compensate for the different internal delays in the pseudorange measurements through the GLONASS receiver, associated to the different frequencies used by the different satellites. Otherwise the station clock estimation would not be coherent with the pseudoranges. It has been observed that in GPS data this effect is much smaller and therefore negligible, normally it is not necessary to estimate such an inter-channel bias for GPS data.

The real-time orbits and clocks are available as a data stream to real-time processing algorithms (such as real-time PPP), and stored in standard formats (SP3, clock RINEX) for offline use.

The quality of the products is monitored by performing comparisons of the overlapping solutions, and by calculating at regular intervals a PPP solution of five control stations of known coordinates. When the quality of the most recent solution is considered insufficient, a prediction from the previous one is used instead, until a new valid solution is available. In addition, the products are also compared to the IGS solutions when they are available. The comparison of real-time solutions with the IGS Rapid products is shown in Figure 4.

The typical value for orbits (3D RMS for all satellites, read on the left y-scale) is around 6cm, and for clocks (read on the right y-scale) it is around 0.3 ns.

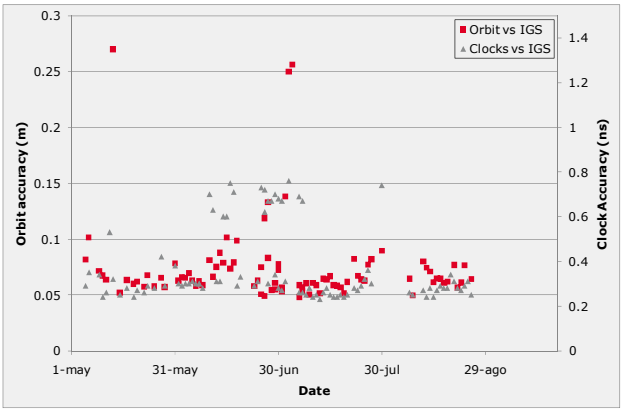

Figure 4: Performances of Real Time GPS Products

As is also represented in Figure 2, there is also another ODTS process running in off-line post-processing mode with a latency of 2 days and specific setup, which allows the generation of more precise products. When available, such products are then used for off-line PPP in replacement of the ones generated previously in real time. The comparison of the off-line products with the IGS for a typical day is show in Figure 5. In this case the typical orbit performances are better than 3cm, and clock accuracy is around 0.1ns.

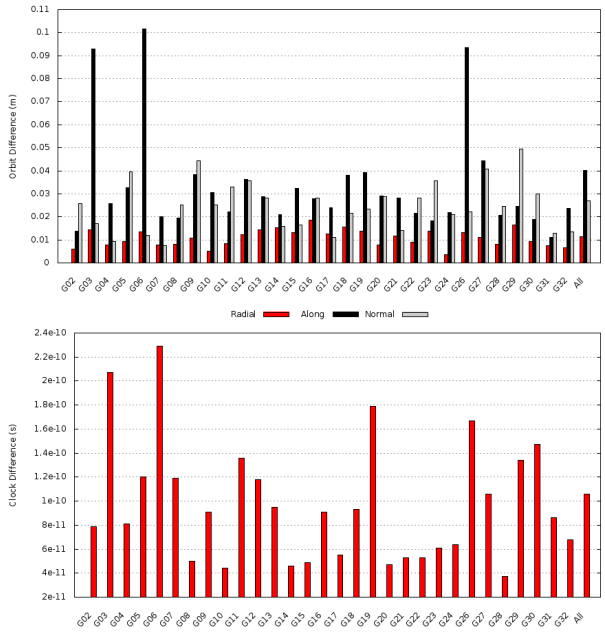

Figure 5: Example performances of off-line GPS Products

The performances of the GLONASS products are shown in Figure 6. Orbit performances (again, 3D RMS for all satellites) are given in terms of overlaps (available after each ODTS) and comparisons with IGS orbits (available with 2-week delay for GLONASS), and read in the left y-scale. The typical value is below 5 cm. Clock performances are given in terms of overlaps only, since the IGS does not currently publish GLONASS clocks. The typical value ranges between 0.1 and 1 ns, and varies notably from day to day. The reason is the estimation of the inter-channel biases, which are correlated with the clocks and therefore make the estimations less stable. However, there is no impact on positioning performances as every solution is always consistent.

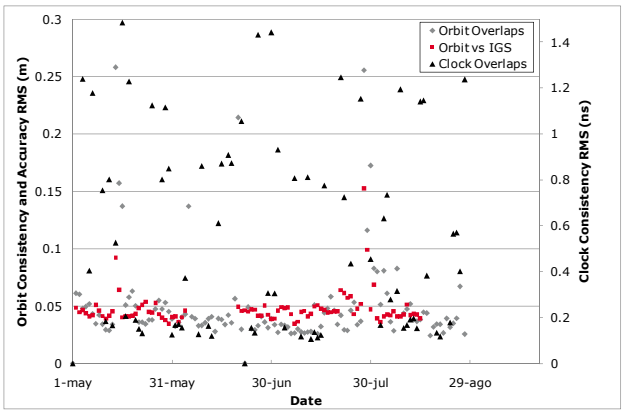

Figure 6: Performances of GLONASS Products

PPP PERFORMANCE

Figure 7 presents the positioning performances of PPP at several IGS stations of known coordinates, when the observation time is 1 day. It can be seen that the accuracy of the PPP solution (vs the coordinates published by the IGS) is around 1 cm, both for GPS and GPS+GLONASS. This test illustrates the good quality of the reference products (both for GPS and for GLONASS) as well as the level of performances of the PPP algorithm.

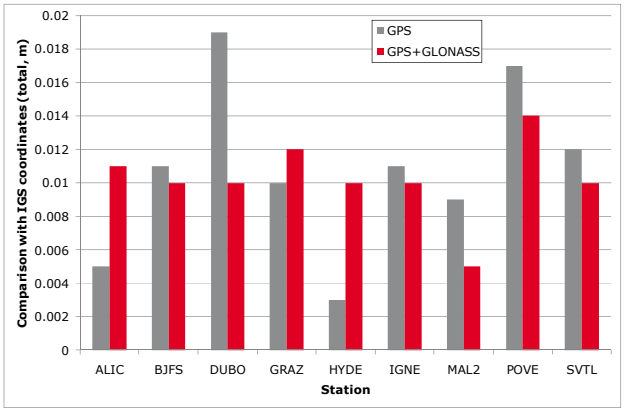

Figure 7: Static PPP Performances (24-hours)

An observation time of 24 hours is adequate for a high accuracy post-processing solution, but is not very suited to field measurement, where shorter measurement intervals would be more practical. Figure 8 shows the performances of Static PPP of one IGS station selected as test user (GLSV), for different observation times ranging from 1 to 24 hours. The results for GPS-only and GPS+GLONASS are shown together for comparison. It can be clearly seen that there is a benefit from longer observation time with a significant improvement after 3 hours. For 1-hour observation time, there is also a significant improvement coming from the multisystem configuration.

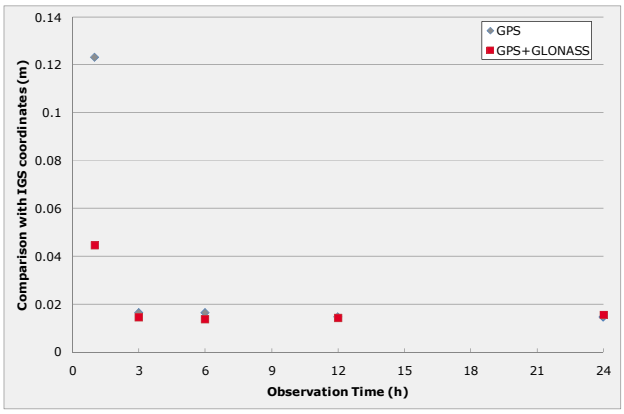

Figure 8: Static PPP Performances at GLSV

In the following example, PPP with 1-hour observation time performances are presented for the test station GLSV, considering the 1-hour observation intervals starting at different times of the same day. It can be seen that when the observation time is short, GPS+GLONASS improves significantly the repeatability of the results, thus providing more stable results along time.

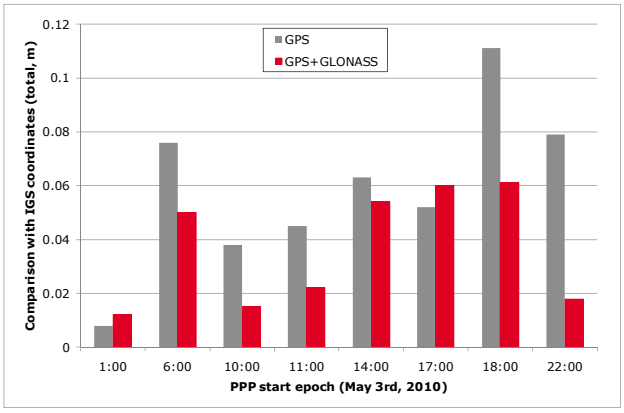

Figure 9: Repeatability of 1-hour PPP solutions at GLSV

The previous results present multi-system PPP as an interesting option for precise positioning, since sub-dm accuracy (sometimes much better) can be reached with 1-hour observation time. The latency with which the solution can be obtained depends only on the latency of the reference products. Real-time generation of products implies that the solution is available immediately after the collection of the measurements (the PPP processing time is almost negligible).

The main application of real-time PPP, however, is kinematic positioning. A kinematic version of *magicGNSS*' PPP algorithm is under development. The initial version, already available, supports only off-line processing. A real-time version is planned for the coming months.

In order to evaluate the performances, a receiver was installed on the roof of a van, and data were recorded during a 30-min drive in Tres Cantos' surrounding countryside. The data (GPS only in this case) were then processed off-line with the new kinematic PPP and compared with a reference trajectory. This reference path was calculated with RTK, using a reference station installed at GMV premises (a few km away). The difference between the solutions versus time (over the 30-min drive) is shown in Figure 10.

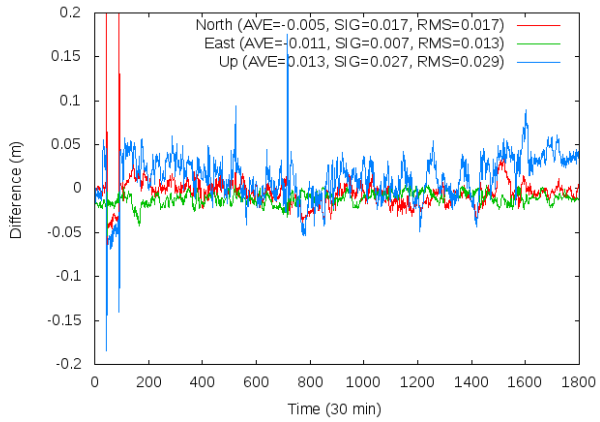

Figure 10: Kinematic PPP vs RTK solutions

The results match up to a few cm. Additional tests in more challenging visibility conditions and with other type of users (e.g. flight trajectories) are currently on-going, with very promising results as well. It is expected that the addition of GLONASS will improve the performances in more challenging visibility conditions.

STATIC IBPL SCENARIO

In order to evaluate the IBPL algorithm using GPS+GLONASS we have used a Topcon Hyper dual-frequency receiver, shown in Figure 11. This is a surveying class portable receiver that can be mounted on a tripod or on a magnetic base for a car roof. This flexible setup allows carrying out static and kinematic tests in different scenarios. The receiver records observations in its internal memory, which are then converted to RINEX format and processed in PPP/IBPL.

Figure 11: Topcon Hyper receiver

Static, open-sky GPS+GLONASS measurements were recorded during around one week on the roof of the GMV building near Madrid, Spain (July 20-26, 2010). The results are shown in the following figures.

Figure 12 represents the horizontal position error distribution. The position error is the difference between the standalone code-based user position and the precise position from PPP (considered as *truth*).

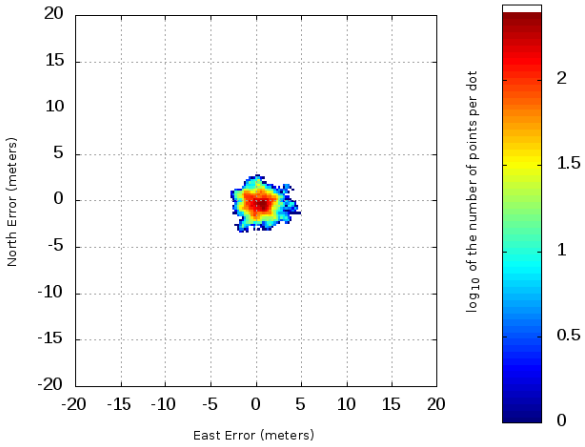

Figure 12: Horizontal position error distribution

Figure 13 shows the evolution in time for the horizontal error (in grey) and Protection Level (in red), for an integrity risk $\alpha = 10^{-4}$ (this means a probability of integrity failure of 0.01%). Figure 14 is the equivalent one for the vertical error.

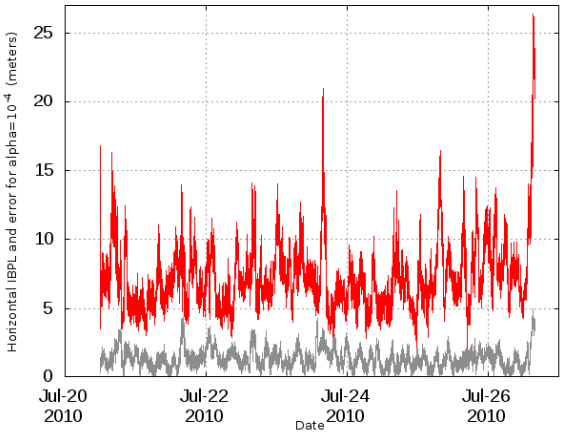

Figure 13: Horizontal error and PL versus time

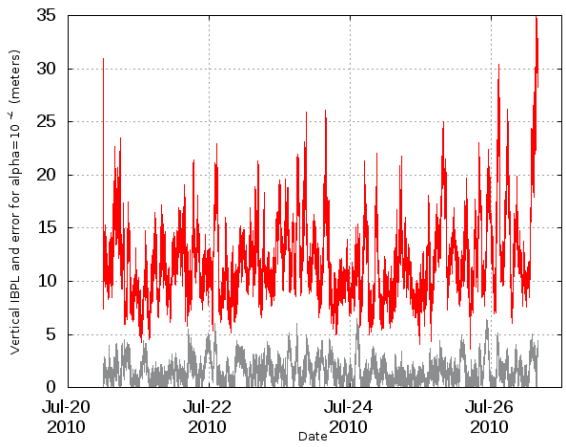

Figure 14: Vertical error and PL versus time

Notice than during the 7 days the PL is nearly always larger than the position error. This means that the PL effectively overbounds the user error, within the given integrity risk. This is in fact better observed on the horizontal and vertical Stanford diagrams shown in Figure 15 and Figure 16, respectively. The horizontal results show that the integrity fails around 0.02% of the time, as compared to an a-priori failure probability of 0.01%. No integrity failure is observed in the vertical component.

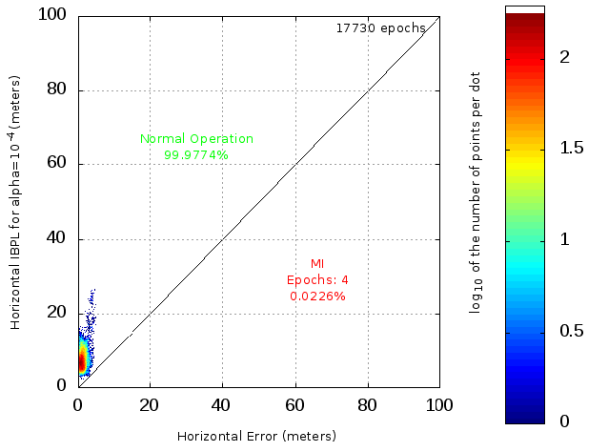

Figure 15: Stanford diagram (Horizontal) for $\alpha = 10^{-4}$

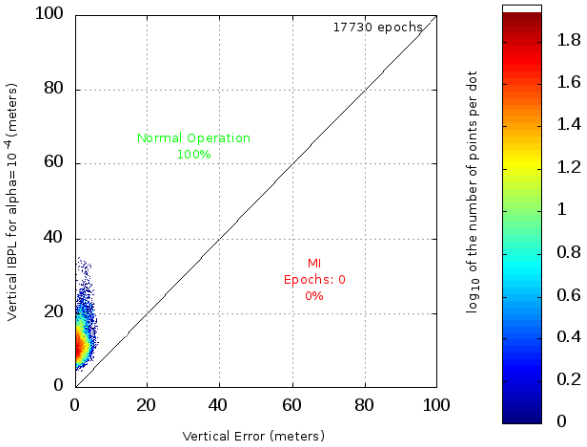

Figure 16: Stanford diagram (Vertical) for $\alpha = 10^{-4}$

Figure 17 shows the accumulated Protection Level histograms corresponding to this static scenario, for all integrity risks ranging from $\alpha = 10^{-1}$ to $\alpha = 10^{-7}$. Naturally, the size of the PL increases as the integrity risk decreases. For example, for $\alpha = 10^{-7}$, 80% of the time the PL is smaller than 20 m, but for $\alpha = 10^{-4}$, 80% of the time the PL is smaller than only 10 m. Figure 18 shows the corresponding histograms for the vertical component.

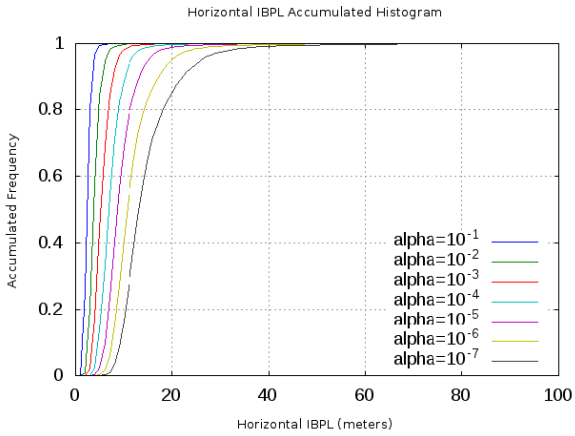

Figure 17: Horizontal PL histograms

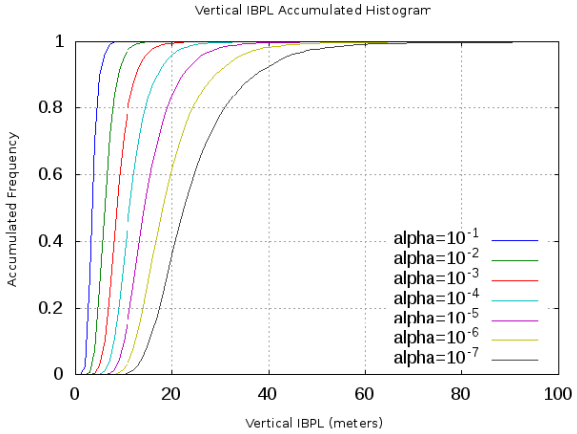

Figure 18: Vertical PL histograms

For comparison, the IBPL results have been recalculated using GPS only, without using the GLONASS measurements. The corresponding accumulated PL histograms are shown in Figure 19 and Figure 20. By comparison to Figure 17 and Figure 18, the reduction of PL size when using GPS+GLONASS is quite dramatic with respect to the GPS-only solution.

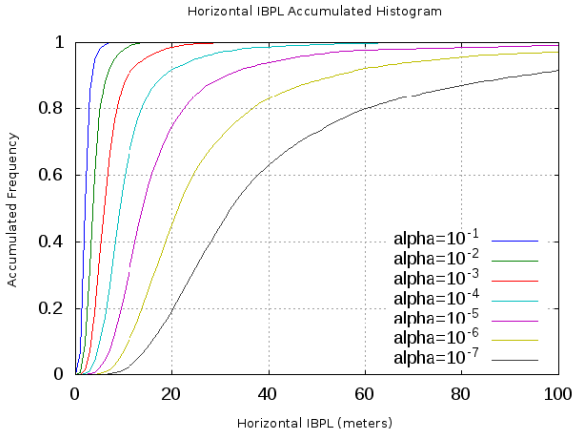

Figure 19: Horizontal PL histograms (GPS-only)

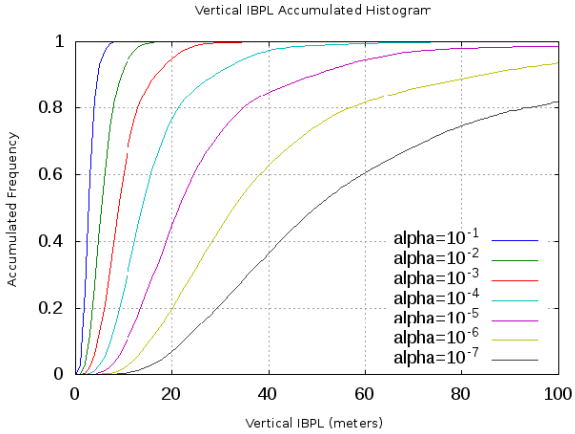

Figure 20: Vertical PL histograms (GPS-only)

KINEMATIC IBPL SCENARIO

In order to evaluate the IBPL concept in a kinematic scenario, our Topcon Hyper receiver was mounted on the roof of a van and taken on a circular tour in an open-sky environment near GMV offices in Madrid. The loop is shown in Figure 21. The duration of the test was around 30 minutes, with a driving distance of around 2.5 km.

Figure 21: Test route for kinematic IBPL

The collected GPS+GLONASS data in RINEX format was processed in PPP/IBPL. The reference trajectory calculated by PPP (*truth*) is estimated to have a 2-cm horizontal error and a 3-cm vertical error (RMS).

Figure 22 shows the evolution in time for the horizontal error (in grey) and Protection Level (in red), for an integrity risk $= 10^{-4}$, over the 30-min route. Figure 23 is the equivalent one for the vertical error. By comparison to Figure 13 and Figure 14, it turns out that the PL size and position error overbounding characteristics are similar in the kinematic and static scenarios.

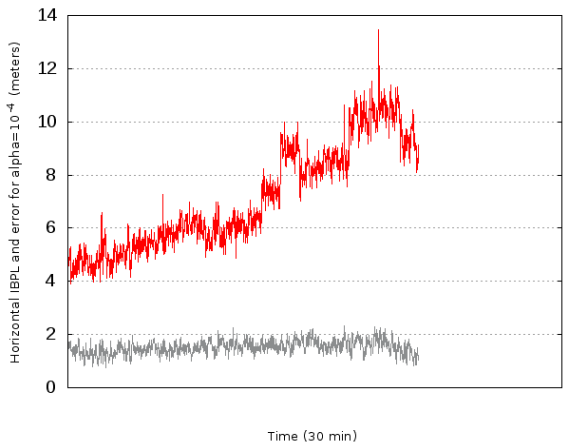

Figure 22: Horizontal error and PL versus time

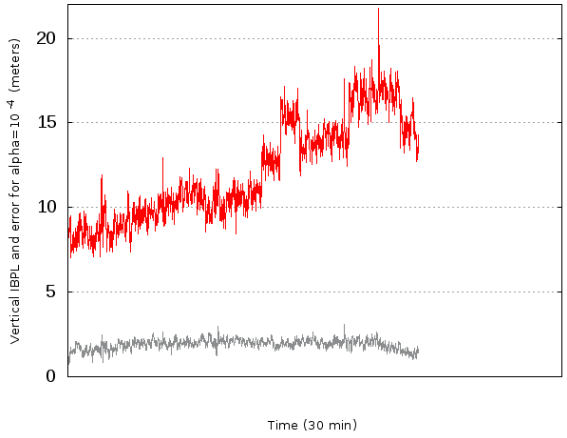

Figure 23: Vertical error and PL versus time

The corresponding horizontal and vertical Stanford diagrams shown in Figure 24 and Figure 25, respectively. No integrity failures are observed in the horizontal or vertical components during the test, as compared to an a-priori failure probability of 0.01% ($\alpha = 10^{-4}$).

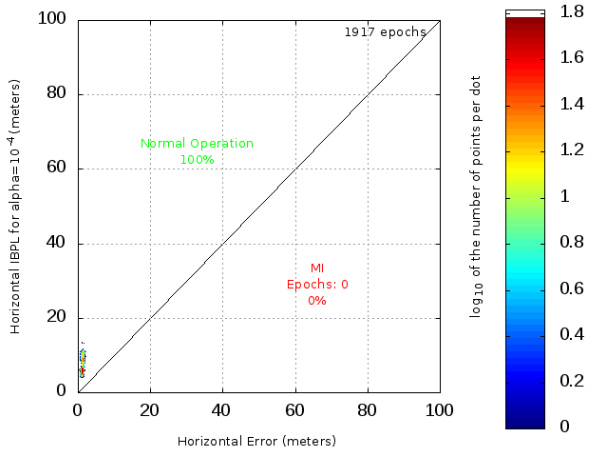

Figure 24: Stanford diagram (Horizontal) for $\alpha = 10^{-4}$

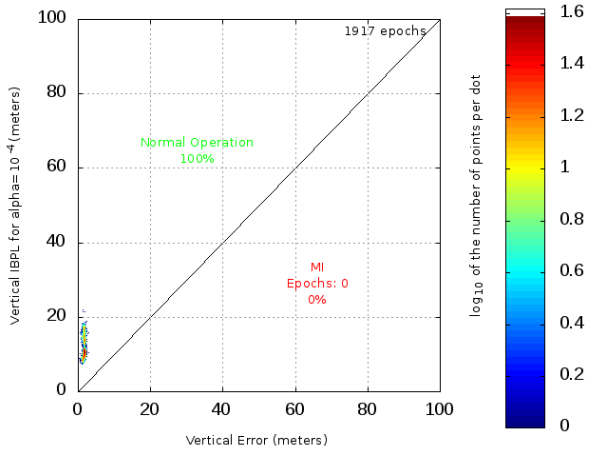

Figure 25: Stanford diagram (Vertical) for $\alpha = 10^{-4}$

Figure 26 shows the accumulated Protection Level histograms corresponding to this kinematic scenario, for all integrity risks ranging from $\alpha = 10^{-1}$ to $\alpha = 10^{-7}$. Figure 27 the corresponding histograms for the vertical component. By comparison to Figure 17 and Figure 18, it turns out that the PL sizes and histogram patterns are similar in the kinematic and static scenarios.

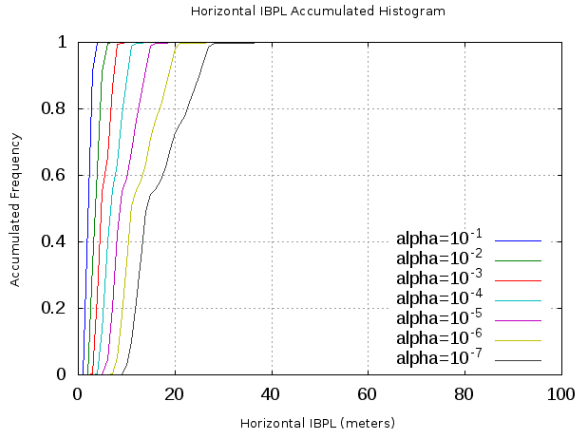

Figure 26: Horizontal PL histograms

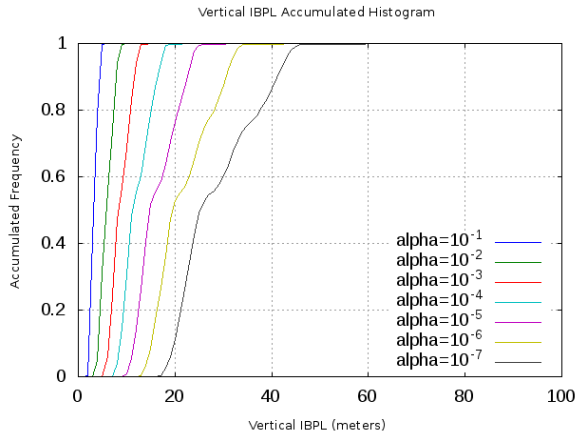

Figure 27: Vertical PL histograms

LONG-TERM STATIC IBPL SCENARIO

A final test has been carried out to test the IBPL performance in a long-term static scenario. For this purpose 200 days of measurements were processed from the WTZR station in Germany. RINEX data rate is 30 sec, which gives more than half a million position samples over the 200 observation days.

As an example let us analyze integrity risks 10^{-5} and 10^{-6}. For a $\alpha = 10^{-5}$ one would a priori expect around 5 integrity failures over the half-million position instances. For a $\alpha = 10^{-6}$ zero or one integrity failure could be expected. The actual processing results are shown in Figure 28 to Figure 31. The a posteriori figures show 1 and 12 integrity failures for $\alpha = 10^{-5}$ in the horizontal and vertical components, respectively, and no integrity failures for $\alpha = 10^{-6}$. PL accumulated histograms (not shown here) present similar patterns to the short-term cases presented above, with horizontal PLs smaller than 20 m 80% of the times even for $\alpha = 10^{-7}$.

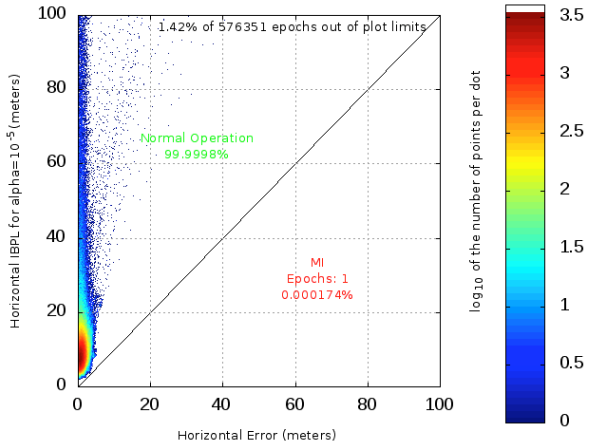

Figure 28: Long-term Stanford diagram (Horizontal) for $\alpha = 10^{-5}$

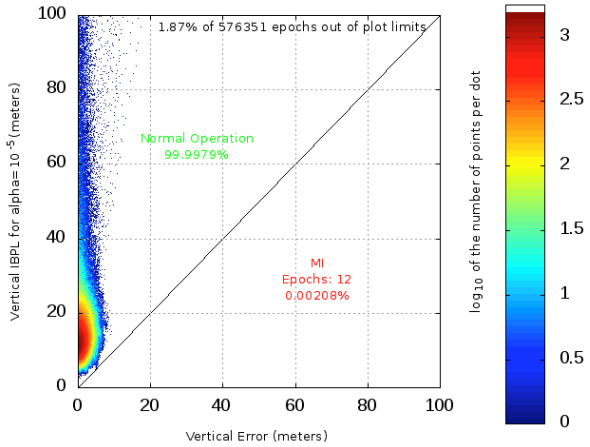

Figure 29: Long-term Stanford diagram (Vertical) for $\alpha = 10^{-5}$

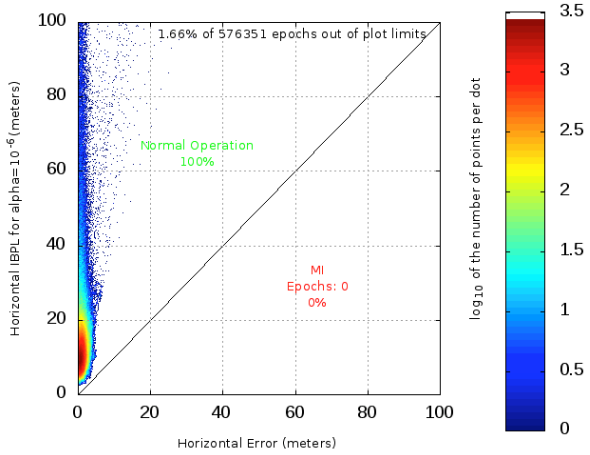

Figure 30: Long-term Stanford diagram (Horizontal) for $\alpha = 10^{-6}$

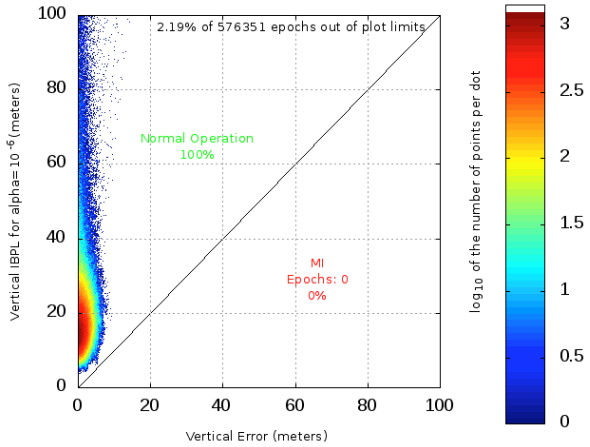

Figure 31: Long-term Stanford diagram (Vertical) for $\alpha = 10^{-6}$

INTEGRATION IN MAGICGNSS

In 2008 GMV introduced *magicGNSS*, a web application for high-precision GNSS data processing [5], [6]. *magicGNSS* is available at http://magicgnss.gmv.com.

The integration of the IBPL and PPP concepts based on RINEX file processing is very convenient and powerful for autonomous integrity demonstration and validation. On one side, PPP allows calculating the *true* position of any single receiver, with a cm-level error, anywhere on the world. The knowledge of the *true* position allows calculating the actual error in the single-frequency pseudorange-based stand-alone position.

By comparing the instantaneous protection levels coming from IBPL with the actual position error, one can generate long-term statistics about integrity performances. Since the combined technique is autonomous and global, the only necessary inputs are dual-frequency RINEX measurement files from a static receiver located anywhere. This allows testing and validating the IBPL concept in many different scenarios, for example in environments of reduced satellite visibility, or in countries with a high ionospheric activity.

The IBPL module implemented in *magicGNSS* allows processing past and recent data from 30 selected GPS+GLONASS core stations from IGS, located worldwide. The user can also upload RINEX files via web of ftp and thus compute IBPL for his own static receiver/station. PPP is carried out automatically prior to IBPL computations, using the first day of the processing interval. Core station data availability allows processing long-term GPS+GLONASS scenarios and generating integrity statistics since January 1, 2010, until current time. Only static PPP/IBPL is supported at present, kinematic data processing will be supported in the near future.

CONCLUSIONS AND FUTURE WORK

We have shown that using combined GPS+GLONASS data in IBPL much reduces PL sizes as compared to the GPS-only solution.

Precise Point Positioning (PPP) is an effective and convenient way of validating IBPL performance (to calculate the *true* receiver position).

Open-sky GPS+GLONASS IBPL results show promising performances. Tests in urban and other difficult environments are still to be done.

IBPL might be applicable to carrier-phase cm-level positioning (RTK, PPP) for precise-positioning integrity. We intend to explore this possibility in the future.

ACKNOWLEDGMENTS

GPS+GLONASS standalone pseudorange-based solution in IBPL is calculated using RTKLIB developed by Tomoji Takasu (gpspp.sakura.ne.jp/rtklib/rtklib.htm).

REFERENCES

1. Dow, J.M., Neilan, R. E., and Rizos, C., *The International GNSS Service in a changing landscape of Global Navigation Satellite Systems*, Journal of Geodesy (2009) 83:191–198, DOI: 10.1007/s00190-008-0300-3

2. J. Cosmen-Schortmann, M. Azaola-Sáenz, M.A. Martínez-Olagüe, M. Toledo-López, GMV (Spain), *Integrity in Urban and Road Environments and its use in Liability Critical Applications*, IEEE/ION PLANS 2008, Monterrey (CA), May 2008.

3. *Azaola-Sáenz, M.; Cosmen Schortmann, J.; Martínez Olagüe, M.A.; Toledo López, M., GMV Aerospace and Defence S.A. (Spain)*, Isotropy-Based Protection Levels: a Novel Method for Autonomous Protection Level Computation with Minimum Assumptions, NAVITEC 2008, Noordwijk (The Netherlands), Dec 2008.

4. Joaquín Cosmen-Schortmann, Miguel Azaola-Saenz, Autonomous Integrity: *An Error Isotropy–Based Approach for Multiple Fault Conditions*, InsideGNSS, Jan-Feb 2009. http://www.insidegnss.com/auto/janfeb09-azaoli.pdf

5. R. Píriz, A. Mozo, P. Navarro, D. Rodríguez, *magicGNSS: Precise GNSS Products Out of the Box*, ION GNSS 2008.

6. Píriz, R., Calle, D., Mozo, A., Navarro, P., Rodríguez, D., Tobías, G., *Orbits and Clocks for GLONASS Precise-Point-Positioning*, ION GNSS 2009.